

Star Formation History up to $z = 7.4$: Implications for Gamma-Ray Bursts and the Cosmic Metallicity Evolution

Li-Xin Li*

Max-Planck-Institut für Astrophysik, 85741 Garching, Germany

Accepted 2008 May 17. Received 2008 April 07; in original form 2007 October 16

ABSTRACT

The current *Swift* sample of gamma-ray bursts (GRBs) with measured redshifts allows to test the assumption that GRBs trace the star formation in the Universe. Some authors have claimed that the rate of GRBs increases with cosmic redshift faster than the star formation rate, whose cause is not known yet. In this paper, I investigate the possibility for interpreting the observed discrepancy between the GRB rate history and the star formation rate history by the cosmic metallicity evolution, motivated by the observation that the cosmic metallicity evolves with redshift and GRBs prefer to occur in low metallicity galaxies. First, I derive a star formation history up to redshift $z = 7.4$ from an updated sample of star formation rate densities obtained by adding the new UV measurements of Bouwens et al. and the new UV and infrared measurements of Reddy et al. to the existing sample compiled by Hopkins & Beacom. Then, adopting a simple model for the relation between the GRB production and the cosmic metallicity history as proposed by Langer & Norman, I show that the observed redshift distribution of the *Swift* GRBs can be reproduced with a fairly good accuracy. Although the results are limited by the small size of the GRB sample and the poorly understood selection biases in detection and localization of GRBs and in redshift determination, they suggest that GRBs trace both the star formation and the metallicity evolution. If the star formation history can be accurately measured with other approaches, which is presumably achievable in the near future, it will be possible to determine the cosmic metallicity evolution with the study on the redshift distribution of GRBs.

Key words:

cosmology; observations – galaxies: evolution – galaxies: high-redshift – galaxies: starburst – gamma-rays: bursts

1 INTRODUCTION

Since the discovery of the afterglows of gamma-ray bursts (GRBs) and the determination of their redshifts (Metzger et al. 1997; van Paradijs et al. 1997), it has been firmly established that GRBs are at cosmological distances (for recent reviews see Piran et al. 2004; Zhang & Mészáros 2004; Mészáros 2006). Observations on the hosts of GRBs have revealed that long-duration GRBs (hereafter GRBs) are associated with faint, blue and often irregular galaxies with high star formation rates (SFRs) (Conselice et al. 2005; Fruchter et al. 2006; Tanvir & Levan 2007; Wainwright, Berger & Penprase 2007, and references therein), confirming the early speculation that GRBs occur in star-formation regions and arise from the death of massive stars (Paczynski 1998; Wijers et al. 1998; see, however,

Le Floc'h et al. 2006). The discovery of the GRB-supernova connection (Galama et al. 1998; Li 2006; Woosley & Heger 2006, and references therein) supports the collapsar model for long-duration GRBs (MacFadyen & Woosley 1999; MacFadyen, Woosley & Heger 2001).

Because of their very high luminosity, GRBs can be detected out to the edge of the visible Universe with minimal extinction by intervening gases and dust (Ciardi & Loeb 2000; Lamb & Reichart 2000; Bromm & Loeb 2002; Naoz & Bromberg 2007) and are hence an ideal tool for probing the formation rate and the environments of stars at high redshift, the reionization history, as well as the cosmic chemical evolution (Fynbo et al. 2006a; Price et al. 2006; Savaglio 2006; Totani et al. 2006; Bromm & Loeb 2007; Campana et al. 2007; Gallerani et al. 2007; Prochaska et al. 2007). The advantage of GRBs over quasars for probing the high redshift Universe has been discussed by Bromm & Loeb (2007). It

* E-mail: lxl@mpa-garching.mpg.de

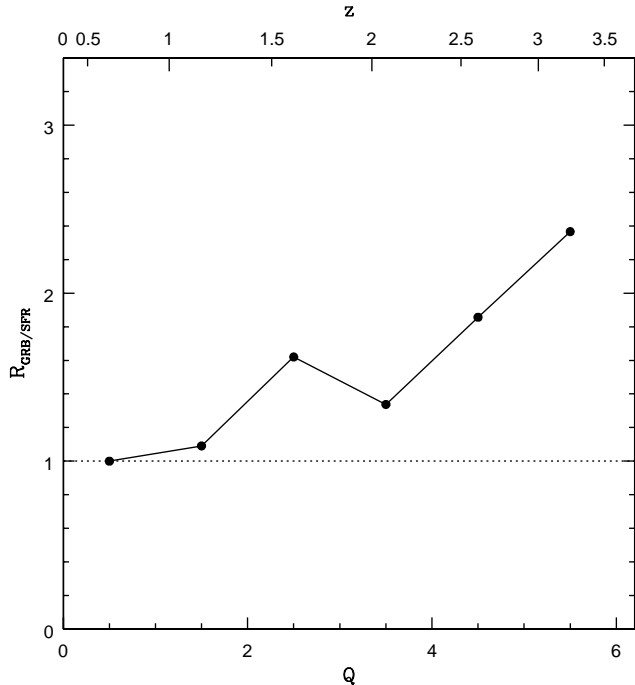


Figure 1. The observed ratio of the GRB rate to the SFR, $R_{\text{GRB/SFR}}$, as a function of $Q(z)$ and z , where $Q(z)$ is defined as an increasing function of redshift z (equation 17 and Fig. 6). Normalization is chosen so that $R_{\text{GRB/SFR}} = 1$ at $Q = 0.5$. The GRB rate history was obtained from a sample of *bright Swift* GRBs so that selection effects are minimized for $z \lesssim 4$ (Kistler et al. 2008, see Section 6.1 of this paper). The SFR is the best fit to an updated sample of measured cosmic SFRs up to $z \sim 7.4$ (eqs. 1 and 2, Section 2). The horizontal dotted line denotes $R_{\text{GRB/SFR}} = 1$, an expected result of the assumption that GRBs trace the star formation unbiasedly.

has also been proposed that GRBs can be used as standard candles to constrain cosmological parameters (Bloom et al. 2003; Friedman & Bloom 2005; Schaefer 2007, and references therein). However, this proposal has been seriously challenged by a recent study of Li (2007).

To study the relation between GRBs and the star formation, people often assume that the GRB rate is proportional to the SFR then compare the predicted distribution of the GRB redshift (or other parameters, e.g. the intensity) to the observed distribution (Totani 1997; Mao & Mo 1998; Wijers et al. 1998; Porciani & Madau 2001; Natarajan et al. 2005; Jakobsson et al. 2006; Daigne et al. 2007; Le & Dermer 2007, for a review see Coward 2007). If GRBs trace the star formation in the Universe unbiasedly, one would expect that the ratio of the GRB rate to the SFR ($R_{\text{GRB/SFR}}$) does not vary with redshift. Then, an accurate measurement of the GRB rate history at high redshift would directly lead to the star formation history (SFH) in the early epoch which is otherwise hard to measure with the current technology because of the uncertainty in dust obscuration for UV photons (Hopkins & Beacom 2006).

Unfortunately, recent studies show that GRBs do not seem to trace the star formation unbiasedly (Fig. 1). Based on the current understanding on the SFH and the *Swift* sample of GRBs with measured redshifts, people have

found that $R_{\text{GRB/SFR}}$ increases with redshift significantly (Daigne et al. 2007; Le & Dermer 2007; Kistler et al. 2008; Yüksel & Kistler 2007; Cen & Fang 2008). While observations consistently show that the comoving rate density of star formation is nearly constant in the interval $1 \lesssim z \lesssim 4$ (Hopkins & Beacom 2006), the comoving rate density of GRBs appears evolving distinctly.

Adopting a model-independent approach by selecting bright *Swift* GRBs with the isotropic-equivalent luminosity $L_{\text{iso}} > 10^{51} \text{ erg s}^{-1}$, Kistler et al. (2008) found that there are ~ 4 times as many GRBs at redshift $z \approx 4$ than expected from star formation measurements. They claimed that some unknown mechanism is leading to an enhancement in the observed rate of high-redshift GRBs. With a more sophisticated method, Daigne et al. (2007) found that to reconcile the observed GRB redshift distribution with the measured SFH, the efficiency of GRB production by massive stars would be nearly six to seven times higher at $z \sim 7$ than at $z \sim 2$. Based on their results, Daigne et al. concluded that GRB properties or progenitors must evolve with cosmic redshift.

In this paper, I investigate the relation between the SFH and the GRB rate history, and explore the possibility that the observed enhancement in the GRB rate at high redshift is caused by the cosmic metallicity evolution. Although the possibility of leading to an enhancement in the observed GRB rate evolution by the cosmic metallicity was mentioned by Kistler et al. (2008), they did not give a quantitative analysis or a detailed discussion. Instead, Kistler et al. discussed more thoroughly on other possible causes, including evolution in the fraction of binary systems which had been proposed as a channel for producing GRBs, an evolving initial mass function (IMF) of stars, and evolution in the galaxy luminosity function (LF).

There is growing evidence that metallicities play an important role in the production of GRBs. Observations on the hosts of GRBs revealed that GRBs prefer to occur in galaxies with low metallicities (Fynbo et al. 2003, 2006a; Prochaska et al. 2004; Soderberg et al. 2004; Gorosabel et al. 2005; Berger et al. 2006; Savaglio 2006; Stanek et al. 2006; Wolf & Podsiadlowski 2007; Modjaz et al. 2008; Savaglio, Glazebrook & Le Borgne 2008). Based on the observational and theoretical evidence that the mass-loss rate of Wolf-Rayet stars depends on the metallicity (Crowther et al. 2002; Vink & de Koter 2005; Crowther 2007), theoretical studies on the collapsar model of GRBs arising from single massive stars suggested that GRBs can only be produced by stars with metallicity $Z \lesssim 0.1Z_{\odot}$ since otherwise strong stellar winds will cause stars to lose too much mass and angular momentum to form a disk around a black hole of several solar masses which is essential for the production of GRBs (Hirschi, Meynet & Maeder 2005; Yoon & Langer 2005; Woosley & Heger 2006; Yoon, Langer & Norman 2006).

It is well-known that the cosmic metallicity evolves strongly with redshift, and galaxies at higher redshift tend to have lower metallicities (Pettini et al. 1999; Prochaska et al. 2003; Rao et al. 2003; Kobulnicky & Kewley 2004; Kewley & Kobulnicky 2005, 2007; Kulkarni et al. 2005, 2007; Savaglio et al. 2005, 2008; Wolfe, Gawiser & Prochaska 2005; Savaglio 2006; Péroux et al. 2007). Natarajan et al. (2005) considered a model where GRBs trace the average metallicity in the

Universe rather than the SFR, and the GRB rate decreases with increasing metallicity. However, their model led to a GRB redshift distribution that is nearly indistinguishable from the distribution predicted by the SFR (Jakobsson et al. 2006).

Recently, Langer & Norman (2006) considered the effect of the cosmic metallicity evolution on the integrated production rate of GRBs in the framework of the collapse model, assuming that the GRB rate is jointly determined by the SFR and the metallicity evolution. Adopting a simple model for the metallicity evolution and a best fitted SFR, and assuming that a GRB is produced if a progenitor star is massive enough and has a metallicity below a threshold ($Z \lesssim 0.1Z_{\odot}$), they showed that the observed global ratio of the GRB rate to the core-collapse supernova rate (~ 0.001) can be reproduced. Nuza et al. (2007) and Cen & Fang (2008) investigated the host galaxies of GRBs in a cosmological hierarchical scenario with numerical simulations. They found that the observed properties of GRB hosts are reproduced if GRBs are required to be generated by low metallicity stars.

I will incorporate the model of Langer & Norman (2006) into a probability distribution function of the luminosity and redshift of GRBs to study the rate history of GRBs. For this purpose, I will present an updated SFH obtained by adding the new measurements of SFR densities at $z \sim 2.3$ and 3.05 by Reddy et al. (2008) and at $z \sim 3.8, 5.0, 5.9$ and 7.4 by Bouwens et al. (2007, 2008) to the data compiled by Hopkins & Beacom (2006). With the updated data I will derive an analytic formula for the SFH and show that the observed distribution of *Swift* GRBs can be successfully reproduced when the evolution of the cosmic metallicity is properly taken into account. Then I will argue that, after a significantly expanded and well-defined sample of GRBs with measured redshifts and luminosities is available in future and the SFH at high redshift is accurately determined with other approaches, GRBs will be a powerful tool for probing the cosmic metallicity evolution.

The paper is organized as follows. In Section 2, I present the updated measurements on the SFR up to $z \sim 7.4$ and derive an analytic formula for the cosmic SFH by fitting the updated data. In Section 3, I summarize the current measurements on the evolution of the metallicity in galaxies with cosmic time and argue that the data indicate a consistent picture for the cosmic metallicity evolution when the redshift-dependent relation between the metallicity and the galaxy stellar mass is considered. In Section 4, I describe the *Swift* GRB sample that is used for the current work, show the luminosity distribution of the GRBs, and discuss the selection biases involved in the detection and localization of *Swift* GRBs and the measurement of their redshifts. In Section 5, the model that I adopt for calculating the GRB rate history is outlined, which includes assumptions about the probability distribution function, the SFR, the evolution of cosmic metallicity, and the form of the GRB LF. In Section 6, I present the results calculated with the model, and fit the observed distribution of the luminosity and redshift for the whole GRB sample and a bright GRB subsample. In Section 7, I draw conclusions and discuss some implications of this work.

Throughout the paper, I assume a flat universe with $\Omega_m = 0.3$, $\Omega_{\Lambda} = 0.7$, and $H_0 = 70 \text{ km s}^{-1} \text{ Mpc}^{-1}$.

2 THE UPDATED STAR FORMATION RATE HISTORY

With modern UV and far-infrared (FIR) observations the SFH has been well established for redshift $z \lesssim 4$, with especially tight constraints for $z \lesssim 1$. Hopkins & Beacom (2006) compiled and critically analysed the data that were available then. They found that, despite large data scatter, the SFR in the redshift range of $1 \lesssim z \lesssim 4$ is approximately a constant, which agreed with the previous claim (e.g., Steidel et al. 1999). Beyond $z \sim 4$, although the data were highly incomplete, a meaningful constraint on the SFH was drawn: the SFR declines with $z \gtrsim 4$. From the 120 data points collected from UV, FIR, radio, $H\alpha$ and the Hubble Ultra Deep Field (HUDF) estimates, Hopkins & Beacom (2006) critically selected 56 ‘good’ data points and fitted the SFH with simple analytical formulas and derived conservative uncertainties.¹

For the criteria applied in the selection of ‘good’ data and a complete list of references for the data, please refer to Hopkins & Beacom (2006). Here I update the sample of Hopkins & Beacom (2006) by including the new measurements of Bouwens et al. (2007, 2008) and Reddy et al. (2008).

Using the HUDF and the GOODS fields, Bouwens et al. (2007, 2008) found large samples of star-forming galaxies at $z \sim 4, 5, 6$, and $7-10$. With those data, the rest-frame UV LFs were determined with high accuracies at $z \sim 4-6$. It has been found that the faint-end slope α and the normalization factor ϕ^* show very little evolution with cosmic time, but the characteristic absolute magnitude M_{UV}^* brightens considerably from $z \sim 6$ to ~ 4 (by ~ 0.7 mag) (Bouwens et al. 2007). With all available deep optical and near-IR (NIR) data over the two GOODS fields, Bouwens et al. (2008) have also derived a rest-frame UV LF at $z \sim 7.4$, and obtained a constraint on the UV LF at $z \sim 10$. The SFR densities at $z \sim 4-10$ were derived from those UV LFs, confirming that the cosmic SFR density decreases quickly with increasing redshift beyond $z \sim 4$.

Using a large sample of rest-frame UV-selected and spectroscopically observed galaxies in the redshift interval $1.9 \leq z \leq 3.4$ combined with ground-based spectroscopic $H\alpha$ and *Spitzer* MIPS $24 \mu\text{m}$ data, which includes over 2000 spectroscopic redshifts and ~ 15000 photometric candidates in 29 independent fields covering a total area of almost a square degree, Reddy et al. (2008) derived robust measurements of the rest-frame UV, $H\alpha$, and IR LFs at $1.9 \leq z \leq 3.4$. The results indicate that the UV LF undergoes little evolution between $z \sim 4$ and $z \sim 2$. The SFR density at $z = 2.3 \pm 0.4$ and $z = 3.05 \pm 0.35$ was derived from the UV luminosity density and the IR luminosity density respectively, using the Kennicutt (1998) relations and assuming the Salpeter (1955) IMF from 0.1 to $100 M_{\odot}$.

To include the new data points of Bouwens et al. (2007, 2008) and Reddy et al. (2008) into the sample of Hopkins & Beacom (2006), two types of corrections must be considered. First, UV lights are strongly obscured by dust so a dust-obscuration correction factor C_1 must be applied to the SFR density derived directly from the UV luminosity

¹ The number 58 of ‘good’ data points printed in Hopkins & Beacom (2006) was a typo (A. M. Hopkins, private communications).

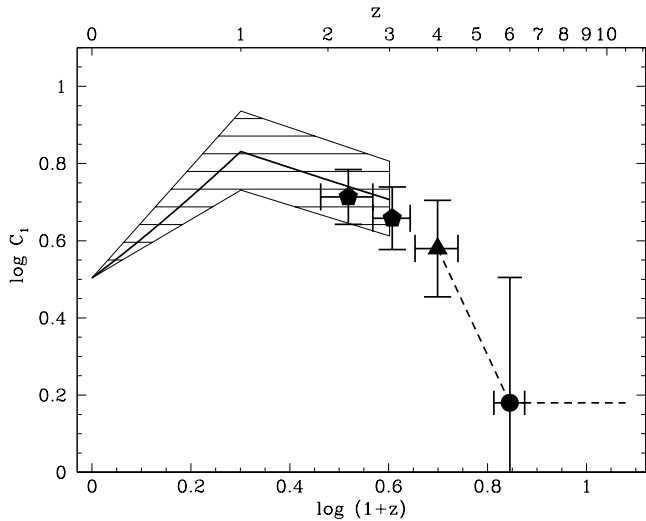


Figure 2. Dust corrections for UV continuum emissions at different redshift intervals. The hatched region is the dust correction obtained from the FIR SFH of Le Floch et al. (2005) ($z < 1$) and the FIR measurements of Pérez-González et al. (2005) ($1 < z < 3$) (see text and Hopkins & Beacom 2006 for details), relative to the UV SFH of Schiminovich et al. (2005). The two pentagons are estimated from the IR and UV SFRs of Reddy et al. (2008), $C_1 \approx 5.17$ at $z \sim 2.3$ and $C_1 \approx 4.55$ at $z \sim 3$. The triangle is the dust correction $C_1 \approx 3.80$ at $z \sim 4$ derived by Ouchi et al. (2004). The circle is the dust correction estimated by Bouwens et al. (2006, 2007), $C_1 \approx 1.51$ at $z \sim 6$. The dashed lines are the linear interpolation between $z = 4$ and $z = 6$, and extension beyond $z = 6$. Note, the dust corrections beyond $z \sim 4$ are highly uncertain.

density. For $z \leq 1$, the FIR SFR density was well measured with *Spitzer* (Le Floch et al. 2005). In Hopkins & Beacom (2006), the UV data at $z \leq 1$ were ‘obscuration corrected’ by adding the FIR SFR density from Le Floch et al. (2005) to each point. For obscuration corrections to the UV data between $z \approx 1$ and $z \approx 3$, Hopkins & Beacom (2006) made use of the fact that the FIR measurements of Pérez-González et al. (2005) are quite flat in this domain as well as being highly consistent with those of Le Floch et al. (2005) at $z < 1$, and add the constant SFR density corresponding to that of Le Floch et al. (2005) at $z = 1$. This looks a reasonable treatment for the obscuration correction at $1 < z < 3$ since later measurements of the IR luminosity density (Caputi et al. 2007; Reddy et al. 2008) agree with a the trend found by Pérez-González et al. (2005) in this redshift range (fig. 27 of Reddy et al. 2008). In addition, the dust corrections derived from the IR and UV SFRs of Reddy et al. (2008) are $C_1 \approx 5.17$ at $z \sim 2.3$ and $C_1 \approx 4.55$ at $z \sim 3$, in good agreement with the values of 4.5–5.0 at $z = 1.0$ –3.5 obtained with other approaches (Steidel et al. 1999; Nandra et al. 2002; Reddy & Steidel 2004).

Beyond redshift $z \approx 3$, dust obscuration is quite uncertain. Investigating the photometric properties of Lyman break galaxies (LGBs) detected in Subaru Deep Field (SDF), Ouchi et al. (2004) estimated the dust extinction of $z \simeq 4$ LGBs and obtained $E(B - V) = 0.15 \pm 0.03$. By the Calzetti et al. (2000) extinction law, this redenning corresponds to a dust correction factor $C_1 \approx 3.80$. The dust extinction at $z \sim 6$ is still unknown. Observing the fact

that the UV continuum slope β at $z \sim 6$ is bluer than that observed at $z \sim 3$ (Stanway, McMahon & Bunker 2005; Yan et al. 2005; Bouwens et al. 2006), Bouwens et al. (2006, 2007) argued that the dust extinction at $z \sim 6$ is lower than that at $z \sim 3$. Adopting $\beta = -2$ (Bouwens et al. 2006) and the extinction- β relation $A_{1600} = 4.43 + 1.99\beta$ (Meurer et al. 1999), Bouwens et al. (2007, 2008) assumed that $C_1 \approx 1.51$ (0.18 dex) at $z \sim 6$ in their SFR derivation. However, comparison of the SFH derived from the Local Group and other nearby galaxies with the cosmic SFH indicates a factor of ~ 10 extinction correction to high-redshift and UV-based SFR measures (Drozdosky et al. 2008).

I will adopt $C_1 \approx 3.80$ at $z \sim 4$, and $C_1 \approx 1.51$ at $z \gtrsim 6$. At $4 < z < 6$, I will follow Bouwens et al. (2007, 2008) and estimate the dust correction by linear interpolation between the $z \sim 4$ and $z \sim 6$ values. The treatment for dust corrections outlined above is sketchedly presented in Fig. 2.

The next correction that should be considered is the factor that converts a ‘partial’ SFR calculated by integration down to a limit luminosity $L_{\min} > 0$ to a ‘total’ SFR calculated by integration down to $L = 0$, which is simply given by $C_2 = \Gamma(2 + \alpha)/\Gamma(2 + \alpha, L_{\min}/L^*)$, where α is the faint-end slope of the Schechter LF, and L^* is the characteristic luminosity. Here $\Gamma(x)$ is the gamma function, and $\Gamma(a, x)$ is the incomplete gamma function.

The ‘partial’ SFR calculated down to the survey magnitude limit is the SFR often reported in the literature. The ‘total’ SFR is strongly dependent on uncertainties in the faint-end slope, but it allows direct comparison with different SFR measurements (Schiminovich et al. 2005). In the compilation of the SFR data in Hopkins & Beacom (2006), it has been attempted to integrate to $L = 0$ in all cases where possible, except for several data points which will be explained and remedied below (A. M. Hopkins, private communications). To add the new data to the sample of Hopkins & Beacom (2006), the integration correction must be made whenever it is relevant.

In the calculation of the integration correction factor C_2 , I make use of the UV LFs derived by Bouwens et al. (2007, 2008) in the redshift interval $4 \lesssim z \lesssim 10$. Since the faint-end slope α of the LFs shows very little evolution with z , a mean value of -1.71 is used in all calculations.

The new data of Bouwens et al. (2008) and Reddy et al. (2008), with the above corrections being applied, are added to the ‘good’ data compiled by Hopkins & Beacom (2006) and shown in Fig. 3. Several data points of Hopkins & Beacom (2006) have been modified or removed. Since Bouwens et al. (2006)’s SFR at $z \approx 6$ has been updated to the new measurement by Bouwens et al. (2007, 2008), it has been removed from Hopkins & Beacom (2006)’s sample (then the sample contains 55 data points). The SFRs of Giavalisco et al. (2004) at $z \approx 3.78$ and 4.92 and that of Bunker et al. (2004) at $z \approx 5.9$, all in Hopkins & Beacom (2006)’s sample, were only integrated to a finite L_{\min} ($= 0.2L_{z=3}^*$ and $0.1L_{z=3}^*$, respectively; A. M. Hopkins, private communications). They are updated by including the integration correction and with new dust corrections according to the procedure described above. The SFR of Ouchi et al. (2004) at $z \approx 4.7$ is updated with a new dust correction factor obtained by linear interpolation between $z = 4$ and $z = 6$.

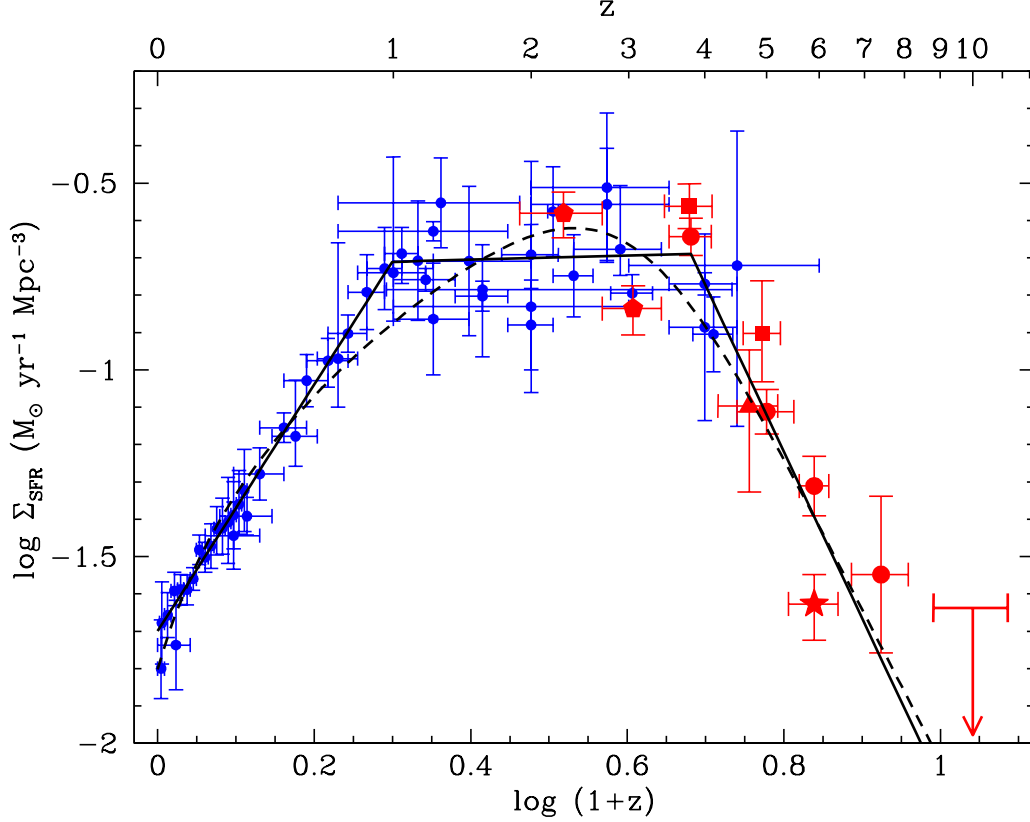


Figure 3. Updated star formation history. The sample contains 51 data points from Hopkins & Beacom (2006) (blue), two UV data points of Giavalisco et al. (2004) with updated corrections (red squares), one UV data point of Bunker et al. (2004) with updated corrections (red star), one UV data point of Ouchi et al. (2004) with updated corrections (red triangle), two UV+IR data points of Reddy et al. (2008) (red pentagons), four UV data points and an upper limit of Bouwens et al. (2008) (red circles and the downward arrow) (see text for details). The total number of data points (not including the upper limit) is therefore 61. The solid black line is the best fit with a piecewise power-law (eqs. 1 and 2), with $\chi_r^2 = 1.18$ (55 degrees of freedom). The dashed black line is the best fit with a formula of Cole et al. (2001) (eq. 3), with $\chi_r^2 = 2.44$ (57 degrees of freedom). In the calculation of chi-squares the errors in z (bin sizes) are not taken into account.

Table 1. The star formation rate density derived from the new UV observational data (Bouwens et al. 2008) and from the old UV data with new corrections (Bunker et al. 2004; Giavalisco et al. 2004; Ouchi et al. 2004)

Reference	Estimator	Redshift	$\log \Sigma_{\text{SFR,un}}^a$	$\log \Sigma_{\text{SFR}}^b$	$\log C_1^c$	$\log C_2^d$
Giavalisco et al. (2004).....	$\sim 1500 \text{ \AA}$	3.780 ± 0.340	-1.639 ± 0.060	-0.562 ± 0.060	0.580	0.496
		4.920 ± 0.330	-1.855 ± 0.140	-0.902 ± 0.140	0.379	0.575
Bunker et al. (2004).....	<i>i</i> -Dropouts	5.900 ± 0.500	-2.301 ± 0.079	-1.627 ± 0.079	0.180	0.494
Ouchi et al. (2004).....	$\sim 1500 \text{ \AA}$	4.700 ± 0.500	-1.521 ± 0.079	-1.097 ± 0.079	0.424	0.000
Bouwens et al. (2008).....	<i>B</i> -Dropouts	3.800 ± 0.300	-1.720 ± 0.050	-0.644 ± 0.050	0.580	0.496
	<i>V</i> -Dropouts	5.000 ± 0.500	-2.050 ± 0.060	-1.112 ± 0.060	0.363	0.575
	<i>i</i> -Dropouts	5.900 ± 0.300	-2.180 ± 0.080	-1.311 ± 0.080	0.180	0.689
	<i>z</i> -Dropouts	7.400 ± 0.700	-2.580 ± 0.210	-1.548 ± 0.210	0.180	0.852
	<i>J</i> -Dropouts	10.00 ± 1.200	< -2.760	< -1.638	0.180	0.942 [†]

^aUncorrected SFR density $\Sigma_{\text{SFR,un}}$ in units of $M_{\odot} \text{ yr}^{-1} \text{ Mpc}^{-3}$.

^bDust and integration corrected SFR density, $\Sigma_{\text{SFR}} = C_1 C_2 \Sigma_{\text{SFR,un}}$, in units of $M_{\odot} \text{ yr}^{-1} \text{ Mpc}^{-3}$.

^cDust correction factor C_1 . At $z \sim 4$, I adopt $C_1 = 3.80$ (Ouchi et al. 2004). At $z \gtrsim 6$, I adopt $C_1 = 10^{0.18} = 1.51$ (Bouwens et al. 2007). For $4 < z < 6$, the value of C_1 is obtained by linear interpolation between $z = 4$ and $z = 6$ (Fig. 2).

^dIntegral correction factor C_2 , converting a ‘partial’ SFR defined by integration down to luminosity $L = L_{\text{min}}$ to a ‘total’ SFR defined by integration down to $L = 0$. The UV LFs published in Bouwens et al. (2008) are adopted, with an average faint-end slope $\alpha = -1.71$. For the data of Giavalisco et al. (2004) and Bouwens et al. (2008), $L_{\text{min}} = 0.2L_{z=3}^*$. For the data of Bunker et al. (2004), $L_{\text{min}} = 0.1L_{z=3}^*$. For the data of Ouchi et al. (2004), the $\Sigma_{\text{SFR,un}}$ has already been integrated down to $L = 0$ by Hopkins & Beacom (2006) so $C_2 = 1$.

[†] C_2 : For the upper limit at $z = 10$ of Bouwens et al. (2008), I take the characteristic magnitude $M_{\text{UV}}^* = -19.6$ in the calculation of C_2 .

Table 2. Reddy et al. (2008)’s star formation rate density derived from UV and IR measurements (in $M_{\odot} \text{ yr}^{-1} \text{ Mpc}^{-3}$)

Redshift	$\log \Sigma_{\text{SFR,UV}}^a$	$\log \Sigma_{\text{SFR,IR}}^b$	$\log \Sigma_{\text{SFR}}^c$
2.30 ± 0.40	$-1.294^{+0.045}_{-0.051}$	$-0.674^{+0.068}_{-0.081}$	$-0.581^{+0.057}_{-0.065}$
3.05 ± 0.35	$-1.494^{+0.060}_{-0.070}$	$-0.944^{+0.075}_{-0.090}$	$-0.836^{+0.061}_{-0.071}$

^aUncorrected SFR density derived from the UV luminosity density, integrated down to $L = 0.04L_{z=3}^*$.

^bSFR density derived from the IR luminosity density between 8 and 1000 μm .

^cThe total SFR density obtained by the sum of $\Sigma_{\text{SFR,UV}}$ and $\Sigma_{\text{SFR,IR}}$.

In Fig. 3, all new data (6 points, not counting the upper limit) and updated old data (4 points) are shown with red symbols, and the unchanged data in the sample of Hopkins & Beacom (2006) are shown with blue symbols. The new data are broadly consistent with previous measurements, and extend the sample to higher redshifts (up to $z \approx 7.4$). The new data and the updated old data are listed in Tables 1 and 2. Since Reddy et al. (2008)’s SFRs are determined by combination of UV and IR measurements, no extra dust correction is needed. The UV SFR is obtained by integration down to $0.04L_{z=3}^*$ which is already small enough. Since the UV SFR contributes to the total UV+IR SFR only by a small fraction ($\sim 20\%$), a further integration correction is not necessary. Hence the SFR data of Reddy et al. (2008) are listed in a separated table.

In Fig. 3 and Tables 1 and 2 the Salpeter IMF has been assumed. Conversion of SFH estimates to an alternative IMF assumption corresponds to a simple scale factor, as described by Hopkins & Beacom (2006).

For the latter application, the SFH presented in Fig. 3 is fitted by a piecewise power-law, as was did in Hopkins & Beacom (2006). The results are

$$\log \Sigma_{\text{SFR}}(z) = a + b \log(1 + z), \quad (1)$$

where

$$(a, b) = \begin{cases} (-1.70, 3.30), & z < 0.993 \\ (-0.727, 0.0549), & 0.993 < z < 3.80 \\ (2.35, -4.46), & z > 3.80 \end{cases}, \quad (2)$$

and Σ_{SFR} is in units of $M_{\odot} \text{ yr}^{-1} \text{ Mpc}^{-3}$. The reduced chi-square of the fit is $\chi_r^2 = 1.18$ (55 degrees of freedom; errors in z not counted). The value of χ_r^2 indicates that the fit is good.

The SFH is also fitted with a formula of Cole et al. (2001)

$$\Sigma_{\text{SFR}}(z) = \frac{a + bz}{1 + (z/c)^d}. \quad (3)$$

The results are $(a, b, c, d) = (0.0157, 0.118, 3.23, 4.66)$, with $\chi_r^2 = 2.44$ (57 degrees of freedom).

Compared to the fit results of Hopkins & Beacom (2006), the updated sample leads to a flatter SFH at $1 \lesssim z \lesssim 4$, and a less rapidly decreasing SFH at $z \gtrsim 4$. A major reason for the large difference in the fitted high- z slope (~ -4 versus ~ -8) is that in Hopkins & Beacom (2006) the SFR density of Bunker et al. at $z = 5.9$ has been underestimated by a factor ~ 3 since it has been integrated only down to $L_{\text{min}} = 0.1L_{z=3}^*$. However, it should be stressed

that at $z \gtrsim 4$ the data suffer large uncertainties due to the lack of knowledge in dust obscuration as explained above.

3 THE COSMIC METALLICITY

Observations have shown that the metallicity in the Universe evolves with cosmic time: the metallicity abundances in galaxies decrease with increasing redshift. This is in agreement with the hierarchical scenario of structure formation, in which metals are assumed to be produced by the formation of stars, injected into the interstellar medium (ISM) by supernova explosions, and some of the metals are expelled from the host galaxy by supernova-driven galactic winds. However, measurements of the cosmic metallicity evolution with different approaches do not appear to converge, and numerical simulations of galaxy formation are still not sufficient for fully reproducing the observations on the cosmic metallicity evolution (Nagamine, Springel & Hernquist 2004; Kobayashi, Springel & White 2007).

Metallicities in damped Ly α absorbers (DLAs) in the spectra of background QSOs have been extensively studied (Pettini et al. 1999; Prochaska et al. 2003; Rao et al. 2003; Kulkarni et al. 2005; Wolfe et al. 2005). The data consistently suggest that the metallicity in QSO-DLAs evolves with cosmic time according to $Z/Z_{\odot} \propto 10^{-\gamma z}$, with $\gamma \approx 0.2-0.4$ (Prochaska et al. 2003; Nagamine et al. 2004; Kulkarni et al. 2005, 2007; Savaglio 2006; Péroux et al. 2007). In addition, there is evidence indicating that the metallicity in sub-DLAs (absorbers with H I column density $N_{\text{HI}} < 10^{20.3} \text{ cm}^{-2}$) evolves with redshift more strongly than that in normal DLAs (with $N_{\text{HI}} > 10^{20.3} \text{ cm}^{-2}$), and are more metal-rich (Kulkarni et al. 2007; Péroux et al. 2007).

DLAs have also been observed in the afterglows of GRBs, indicating metallicities and column densities that are generally higher than in QSO-DLAs (Vreeswijk et al. 2004; Berger et al. 2006; Prochter et al. 2006; Savaglio 2006; Sudilovsky et al. 2007; Watson et al. 2007; Fynbo et al. 2008). A system study on GRB-DLAs (Savaglio 2006) indicates that the metallicity in GRB-DLAs evolves with redshift with a slower rate ($\gamma \approx 0.18$) than that in QSO-DLAs, suggesting that GRB-DLAs and QSO-DLAs belong to two different classes of absorbers although they both trace the ISM in high-redshift galaxies.

By measuring nebular oxygen abundances for 204 emission-line galaxies with redshifts $0.3 < z < 1.0$ in the Great Observatories Origins Deep Survey-North (GOODS-N) field, Kobulnicky & Kewley (2004) found that the metallicity in galaxies with $-18.5 < M_B < -21.5$ evolves with $\gamma \approx 0.14$ from $z = 0$ to 1. Compilation of oxygen abundances in star-forming galaxies with $M_B < -20.5$ and $0 < z < 3.5$ indicates that the metallicity in star-forming galaxies evolves with $\gamma \approx 0.15$ in the redshift range of $0 < z \lesssim 3$ (Kewley & Kobulnicky 2005, 2007).

Different types of metallicity measurements suffer different selection biases so the fact that the values of γ do not converge is probably not surprising. Detection of absorption lines in the neutral ISM of galaxies acrossing QSO sight-lines gives information of one line of sight in the galaxy so the result suffers large statistical fluctuations. Detecting emission lines in the integrated galaxy spectra is observationally challenging at high redshift since prominent lines get

very weak and redshifted to the NIR range (Savaglio et al. 2005). The different evolution observed for QSO-DLAs and GRB-DLAs may indicate that GRB-DLAs are associated with more massive galaxies, on average as massive as the LMC (Savaglio 2006). Reconciling the metallicity distribution of GRB-DLAs, QSO-DLAs, and Lyman-break galaxies (star-forming galaxies) at high redshift has recently been discussed by Fynbo et al. (2008).

It is well-known that the stellar mass of star-forming galaxies is correlated with the metallicity: galaxies with larger stellar masses tend to have higher metallicities (the mass-metallicity relation, Savaglio et al. 2005; Erb et al. 2006; Kewley & Ellison 2008, and references therein). Savaglio et al. (2005) derived a simple relation that gives the metallicity in the gas of a galaxy at a given stellar mass and Hubble time (their eq. 11). With this relation, Savaglio (2006) argued that the apparent difference in the values of γ for QSO-DLAs and GRB-DLAs may be explained by the mass-metallicity relation with the assumption that different measurements probe galaxies with different stellar masses.

Using the scaling $12 + \log(\text{O}/\text{H}) = \log(Z/Z_\odot) + 8.69$ (Savaglio 2006), Savaglio's relation can be written as

$$\begin{aligned} \log(Z/Z_\odot) = & -16.28 + 2.53 \log M - 0.0965 \log^2 M \\ & + 5.17 \log t_H - 0.394 \log^2 t_H \\ & - 0.403 \log t_H \log M, \end{aligned} \quad (4)$$

where M is the stellar mass in units of M_\odot , and t_H is the Hubble time in units of Gyr.

The relation was used to fit the evolution of the metallicity in QSO-DLAs and GRB-DLAs. It was predicted that the stellar mass of QSO-DLAs is $10^{8.82 \pm 0.65} M_\odot$ (Savaglio et al. 2005), and the stellar mass of GRB hosts is preferably in the range of $10^{8.6} - 10^{9.8} M_\odot$ (Savaglio 2006). The latter is in agreement with the average stellar mass of $10^{9.3} M_\odot$ with a $1-\sigma$ dispersion of 0.8 dex found for 46 GRB hosts with optical-NIR photometry and spectroscopy (Savaglio et al. 2008).

With a galaxy stellar-mass function $\Phi(M)$, two average metallicities can be defined. The first one is defined by averaging over the number of galaxies

$$\left\langle \frac{Z}{Z_\odot} \right\rangle_1 \equiv \frac{\int_{M_{\min}}^{\infty} Z \Phi(M) dM}{Z_\odot \int_{M_{\min}}^{\infty} \Phi(M) dM}. \quad (5)$$

For a Schechter function of galaxy stellar-masses (Panter, Heavens & Jimenez 2004), the low-mass-end slope α is usually < -1 . Then, the integral of $\Phi(M)$ over M does not converge as the lower limit of the integral goes to zero. Hence, a non-zero minimum stellar mass M_{\min} is necessary in the definition of $\langle Z/Z_\odot \rangle_1$.

The other average metallicity is defined by averaging over the stellar mass (or the mass of H I gases)

$$\left\langle \frac{Z}{Z_\odot} \right\rangle_2 \equiv \frac{\int_0^{\infty} Z M \Phi(M) dM}{Z_\odot \int_0^{\infty} M \Phi(M) dM}, \quad (6)$$

i.e., the total metal mass divided by the total stellar (or H I) mass. In the definition of $\langle Z/Z_\odot \rangle_2$, the lower limit of mass in the integral is set to zero since the integral converges.

Adopting a Schechter function of galaxy stellar-masses from Panter et al. (2004) with $\alpha = -1.16$ and the critical mass $M_* = 7.64 \times 10^{10} h^{-2} M_\odot$ (with $h = 0.7$, h is the

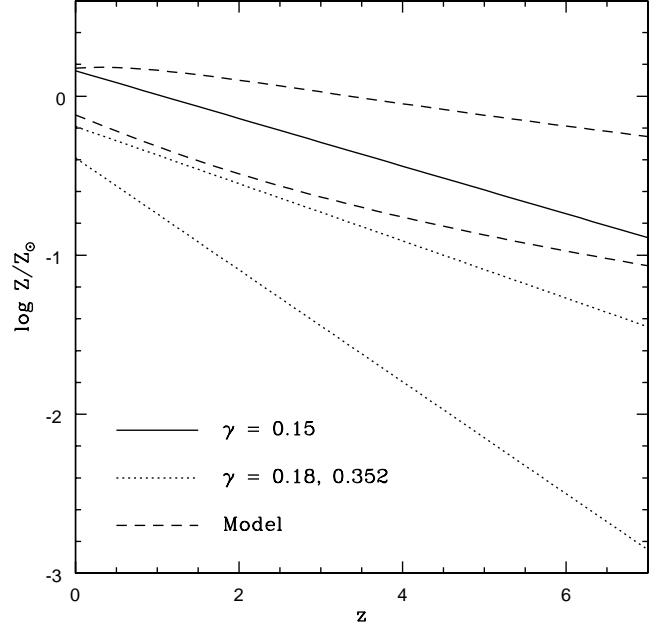


Figure 4. The cosmic metallicity as a function of the redshift. The solid line is the fit to the metallicity in star-forming galaxies by $Z/Z_\odot \propto 10^{-\gamma z}$, with $\gamma = 0.15$ (Kewley & Kobulnicky 2005, 2007). The two dotted lines are the fits to QSO-DLAs with $\gamma = 0.352$ (lower line) and GRB-DLAs with $\gamma = 0.18$ (upper line; Savaglio 2006). The two dashed lines are the average metallicities calculated with the empirical model of Savaglio et al. (2005), $\langle Z/Z_\odot \rangle_1$ (lower line, eq. 5) and $\langle Z/Z_\odot \rangle_2$ (upper line, eq. 6).

Hubble constant in units of $100 \text{ km s}^{-1} \text{ Mpc}^{-1}$), I calculated $\langle Z/Z_\odot \rangle_1$ (with $M_{\min} = 10^{7.5} M_\odot$) and $\langle Z/Z_\odot \rangle_2$ for the metallicity given by equation (4). The results, with comparison to measurements, are shown in Fig. 4.

The $\langle Z/Z_\odot \rangle_1$ defined by equation (5) is suitable for comparison with observations since the observed metallicity evolution is usually derived from the fit to the distribution of metallicity abundances in individual galaxies. From Fig. 4, $\langle Z/Z_\odot \rangle_1$ (the lower dashed line) is between the measured metallicity in star-forming galaxies (with $\gamma = 0.15$, solid line) and that in GRB-DLAs (with $\gamma = 0.18$, upper dotted line).

The $\langle Z/Z_\odot \rangle_2$ defined by equation (6) (or its variant, e.g., ratio of the total mass of metals to the total mass of H I gases in all galaxies) is sometimes adopted in numerical simulations (e.g., Nagamine et al. 2004). From Fig. 4, $\langle Z/Z_\odot \rangle_2$ (the upper dashed line) gives an estimate of the metallicity higher than that derived from the fit to measurements, and evolves with z with a slower rate. This is caused by the fact that, by its definition, the contribution to $\langle Z/Z_\odot \rangle_2$ comes dominantly from galaxies with stellar masses around $M_* \sim 10^{11} M_\odot$ while faster evolution and lower metallicities are attributed to galaxies with smaller stellar masses (Savaglio et al. 2005).

For $\alpha < -1$, the value of $\langle Z/Z_\odot \rangle_1$ and its evolution are sensitive to M_{\min} , since the dominant contribution to the integral comes from low stellar-mass and hence low metallicity galaxies because of their large numbers. The choice of $M_{\min} = 10^{7.5} M_\odot$ seems reasonable according to the measurement on the distribution of stellar masses for GRB host galaxies (Savaglio et al. 2008).

Although Savaglio’s relation leads to reasonable results in fitting the metallicity distribution of QSO-DLAs and GRB-DLAs by varying the stellar mass, its validity and calibration need to be tested and improved with future measurements on metallicity and stellar masses of galaxies. For the purpose of fitting the GRB rate history in this paper, it is enough to adopt an empirical evolution equation

$$Z/Z_{\odot} \propto 10^{-\gamma z} \quad (7)$$

with a constant γ as adopted by Langer & Norman (2006). Given the limit number of GRBs with measured redshifts and spectra and many unknown observational biases, it is impossible to constrain the parameters in the metallicity evolution with GRBs at the present time.

Since long-duration GRBs occurred in star-forming galaxies, following Langer & Norman (2006) I will adopt the value $\gamma = 0.15$ derived by Kewley & Kobulnicky (2005, 2007).

4 THE SWIFT GRB SAMPLE

4.1 The Luminosity Distribution of *Swift* GRBs

Since the launch of *Swift* in late 2004, 310 GRBs have been detected by 31 March 2008, of which 181 bursts have optical detections (by the UV/Optical Telescope on *Swift* and/or ground telescopes) and 102 bursts have measured redshifts.^{2,3}

Butler et al. (2007) have compiled a catalog of 218 *Swift* GRBs and calculated their durations and spectral parameters between and including GRBs 041220 and 070509, including 77 events with measured redshifts. From that catalog, Kistler et al. (2008) selected 63 bursts with long durations ($T_{90} > 2$ s, T_{90} is the observed time duration to contain 90% of the total counts, with 5% in front and the other 5% behind.) and reliable redshift measurements to investigate the redshift distribution of *Swift* GRBs. The following four long GRBs are contained in the catalog of Butler et al. but not included in the sample of Kistler et al., because of their unreliable redshifts: 060116, 060202, 060428B and 061004 (M. D. Kistler, private communications).

Liang et al. (2007) have derived the luminosity for 45 long *Swift* GRBs using the method developed by Zhang et al. (2007b). Cabrera et al. (2007) have published the spectral and energetic results for a smaller sample of *Swift* GRBs, which contains 29 long bursts with calculated isotropic-equivalent energy.

I use the sample of Kistler et al. (2008) selected from Butler et al. (2007)—with addition of GRB 050223—for my analysis, since it is the largest sample to date. The 64 GRBs in the sample have determined durations, redshifts, peak spectral energy, and the isotropic-equivalent energy in the 1–10⁴ keV band in the rest frame of GRBs (Butler et al. 2007; Kocevski & Butler 2007). For the isotropic-equivalent energy E_{iso} , I take the values from the table 1 of Kocevski & Butler (2007) since they have more significant digits than the corresponding values in the table 2 of Butler et al. (2007). However, GRB 050223 (not included

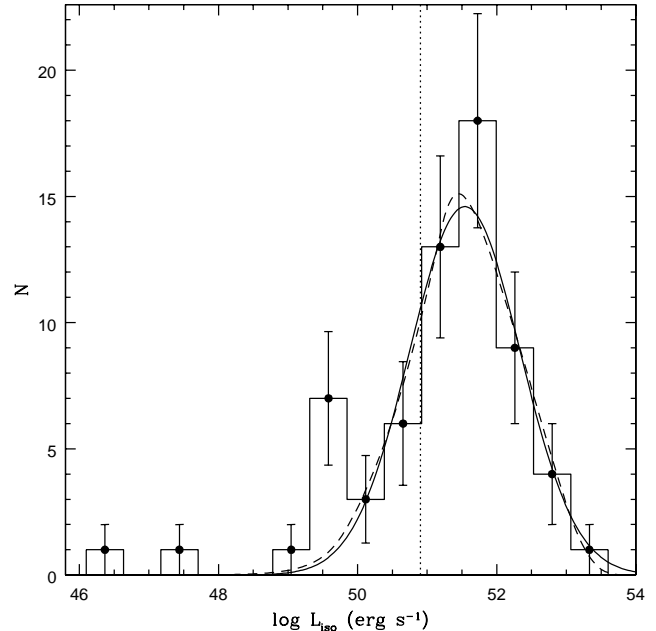


Figure 5. Distribution of the isotropic-equivalent luminosity (defined by eq. 8) for 64 long-duration *Swift* GRBs (the solid line histogram, with the number of GRBs in each bin indicated by a dark point with Poisson error bars). The solid curve is a Gaussian fit to the distribution of $\log L_{\text{iso}}$, with $\chi^2_{\text{f}} = 1.24$. The dashed curve is a least chi-squares fit by the model in Section 5, with $\chi^2_{\text{f}} = 1.18$ (see Sections 5 and 6 for details). The 45 bursts to the right of the vertical dashed line at $E_{\text{iso}} = 0.8 \times 10^{51}$ erg s⁻¹ form a subsample of ‘bright GRBs’, which are not affected by the luminosity threshold when $z < 4$ (Section 6.1).

in Kistler et al. 2008) was not listed in Kocevski & Butler (2007), so I take the value of E_{iso} for this event from Butler et al. (2007).

Following Kistler et al. (2008), I calculate the isotropic-equivalent luminosity of a GRB by

$$L_{\text{iso}} \equiv \frac{E_{\text{iso}}}{T_{90}}(1+z). \quad (8)$$

The distribution of L_{iso} for the 64 GRBs in the sample is shown in Fig. 5, which is fitted by a log-normal distribution with a mean of $\log L_{\text{iso}} = 51.54$ (L_{iso} in erg s⁻¹), a dispersion $\sigma_{\log L_{\text{iso}}} = 0.795$, and $\chi^2_{\text{r}} = 1.24$.

The *Swift* trigger is very complex and the sensitivity of the detector is very difficult if not impossible to parameterize exactly (Band 2006). However, an effective luminosity threshold appears to be present in the data (Kistler et al. 2008, their figure 2). I find that the luminosity threshold can be approximated by a bolometric energy flux limit $F_{\text{lim}} = 1.2 \times 10^{-8}$ erg cm⁻² s⁻¹. The luminosity threshold is then

$$L_{\text{lim}} = 4\pi D_L^2 F_{\text{lim}}, \quad (9)$$

where D_L is the luminosity distance to the burst.

With the above luminosity threshold and an adopted GRB rate history, the observed luminosity distribution can be fitted by an intrinsic Schechter LF with a power-law index -1.225 and a characteristic luminosity 0.986×10^{53} erg s⁻¹ (the dashed line in Fig. 5; for details see Section 6.2).

The data have a moderate excess around $L_{\text{iso}} = 3.8 \times$

² http://swift.gsfc.nasa.gov/docs/swift/archive/grb_table/

³ <http://www.mpe.mpg.de/jcg/grbgen.html>

$10^{49} \text{ erg s}^{-1}$, at the $2.4\text{-}\sigma$ level (relative to the log-normal distribution). It probably indicates the existence of a faint population of GRBs, which will be discussed in details in Section 6.

4.2 Selection Biases

Selection effects involved in a GRB sample are hard to model quantitatively. There are at least two kinds of selection effects at work, which have been extensively discussed in the literature (Bloom et al. 2003; Coward 2007; Fiore et al. 2007; Guetta & Della Valle 2007; Kistler et al. 2008; Le & Dermer 2007; Coward et al. 2008): (1) GRB detection and localization; and (2) redshift determination through spectroscopy/photometry of the GRB afterglow or the host galaxy. A full address of these issues is beyond the scope of this paper, so I only give a brief description on them.

Since all the GRBs in the sample used in this paper (and in Kistler et al. 2008) are detected by Burst Alert Telescope (BAT) onboard *Swift*, biases arising from GRB detection are minimized although the sensitivity of BAT is very difficult to parameterize exactly (Band 2006). An effective luminosity threshold introduced above and in Kistler et al. (2008) would be a reasonable approximation of the detection criteria for the bursts in the sample.

Due to the transient nature of GRBs, a fast and accurate location of the burst is crucial for the determination of the redshift. The automatic slew ability and the multi-wavelength nature of *Swift* have led that an accurate localization of the GRB is possible shortly after its detection, with an efficiency higher than any previous GRB observatory (e.g., *BeppoSAX* and *HETE2*). An impressive number of ground-based facilities (dedicated robotic telescopes, VLT, Gemini, Keck, etc) have been involved in *Swift* follow-up observations. However, optical afterglows have been discovered for only $\sim 50\%$ of *Swift* GRBs, a fraction only slightly greater than that of *BeppoSAX* and *HETE2* samples (Berger et al. 2005; Fiore et al. 2007; Kann et al. 2008). The cause for the non-detection of optical afterglows for well localized GRBs remains a puzzle (Castro-Tirado et al. 2007; Rol et al. 2007; Kann et al. 2008).

Generally, an apparently bright burst would be easier to localize than an apparently faint burst. On average more distant bursts are expected to have lower observed gamma-ray fluxes, hence the number of GRBs with high redshift might have been somewhat underestimated. But this indicates that the deviation of the GRB rate from that predicted by the SFR could be more serious than that has been observed (Kistler et al. 2008).

For the GRBs detected and localized by *Swift*, most of them are followed-up spectroscopically by ground-based telescopes. The participation of ground-based telescopes in follow-up observations has greatly increased the number of GRBs with redshifts (about 1/3 of the total *Swift* GRBs). However, this also makes the selection biases in the redshift determination extremely complex, since instrumental selection biases of different telescopes have to be involved. Different techniques have also been applied in the redshift measurement: absorption lines, emission lines and photometry of the Lyman edge, which causes additional biases.

In addition to the various selection biases in redshift

measurements discussed above, there has been a well-known ‘redshift desert’ in the redshift interval $1.4 \lesssim z \lesssim 2.5$ since galaxies in that range have been hard to detect spectroscopically with traditional ground-based telescopes (Adelberger et al. 2004; Steidel et al. 2004). However, the ‘redshift desert’ problem does not seem to be serious for *Swift* GRBs, since among the 85 long GRBs with measured redshifts by 31 March 2008, 23 bursts are in the redshift interval $1.4 \lesssim z \lesssim 2.5$ (Fig. 11). This is probably caused by the fact that different telescopes have different spectral ranges and they complement each other to some degrees.

5 A MODEL FOR THE GRB RATE HISTORY

There is evidence that GRBs are beamed (Harrison et al. 1999; Kulkarni et al. 1999; Stanek et al. 1999). Hence, when discussing the probability distribution function of GRBs, the effect of jet beaming must be taken into account. Assuming that a GRB radiates its energy into two oppositely directed jets, each having a half-opening angle θ_{jet} . The total solid angle spanned by the jets is then $4\pi\omega$, where the beaming factor $\omega \equiv 1 - \cos\theta_{\text{jet}} < 1$.

For simplicity, I assume that except the comoving rate density, the property of GRBs does not evolve with the cosmic redshift. Then, the intrinsic distribution function of z , L_{iso} and $y \equiv \log(\tan\theta_{\text{jet}})$ must have a form

$$P(z, L_{\text{iso}}, y) = f(z)\phi(L_{\text{iso}})\psi(L_{\text{iso}}, y), \quad (10)$$

where

$$f(z) \equiv \left(\frac{c}{H_0}\right)^{-3} \frac{\Sigma_{\text{GRB}}(z) dV_{\text{com}}}{1+z} \frac{dV_{\text{com}}}{dz}, \quad (11)$$

$(c/H_0)^{-3}\Sigma_{\text{GRB}}(z)$ is the comoving rate density of GRBs, and V_{com} is the comoving volume. Here c is the speed of light.

In equation (10), $\psi(L_{\text{iso}}, y)$ is normalized with respect to y

$$\int_{-\infty}^{\infty} \psi(L_{\text{iso}}, y) dy = 1. \quad (12)$$

In a flat universe ($\Omega_m + \Omega_\Lambda = 1$), the comoving volume is calculated by

$$\frac{dV_{\text{com}}}{dz} = 4\pi D_{\text{com}}^2 \frac{dD_{\text{com}}}{dz}, \quad (13)$$

where the comoving distance

$$D_{\text{com}}(z) \equiv \frac{c}{H_0} \int_0^z \frac{dz'}{\sqrt{\Omega_m(1+z')^3 + \Omega_\Lambda}}. \quad (14)$$

A GRB is detected by an observer only if one of its jets points toward the observer. Hence, without consideration of other selection effects, the probability for a GRB to be detected by an observer is equal to ω . Multiplying equation (10) by ω then integrating it over y , one gets the observed distribution function of z and L_{iso} without considering other selection effects

$$P(z, L_{\text{iso}}) = f(z)\Phi(L_{\text{iso}}), \quad (15)$$

where the beaming-convolved LF

$$\Phi(L_{\text{iso}}) \equiv \langle \omega \rangle \phi(L_{\text{iso}}), \quad \langle \omega \rangle \equiv \int_{-\infty}^{\infty} \omega \psi(L_{\text{iso}}, y) dy. \quad (16)$$

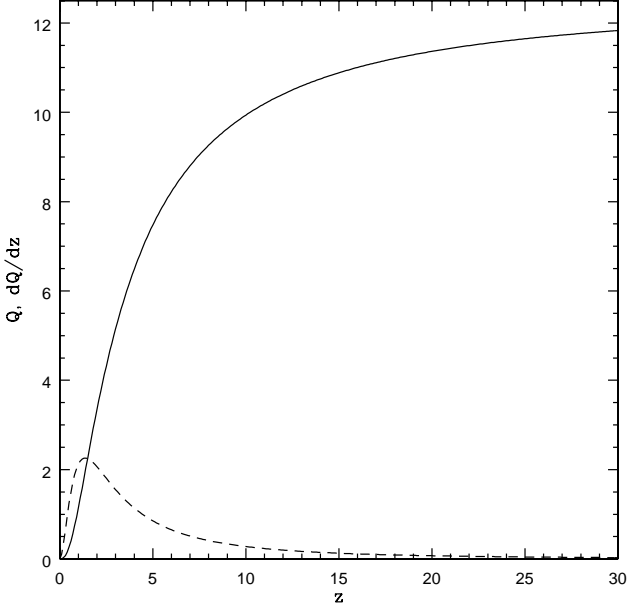


Figure 6. The cosmic volume coordinate Q (defined by eq. 17) as a function of the cosmic redshift z (solid curve), and the derivative dQ/dz (dashed curve). ($\Omega_m = 0.3$, $\Omega_\Lambda = 0.7$.)

Generally, the luminosity-averaged jet beaming factor $\langle \omega \rangle$ is a function of L_{iso} . Therefore, the beaming-convolved LF $\Phi(L_{\text{iso}})$ differs from the intrinsic LF $\phi(L_{\text{iso}})$.

For the purpose of studying the rate density history of GRBs and the star formation, it is more convenient to use a dimensionless volume coordinate Q than to use the redshift z , where $Q = Q(z)$ is defined by (Kistler et al. 2008)

$$Q(z) \equiv \left(\frac{c}{H_0}\right)^{-3} \int_0^z \frac{1}{1+z'} \frac{dV_{\text{com}}}{dz'} dz', \quad (17)$$

which increases monotonically with z (Fig. 6). For $z \ll 1$, one has $Q \approx 4\pi z^3/3$. As $z \rightarrow \infty$, one has $Q \rightarrow \text{constant}$.

The coordinate Q is particularly useful in binning the data since the definition of Q has taken into account both the effect of comoving volume and the effect of cosmic time dilation. For example, if the comoving rate density of GRBs were a constant, in each equally-sized bin of Q the number of GRBs would be a constant. In contrast, if the data are binned with an equal size of Δz , the number of GRBs would change dramatically from bin to bin because of the comoving volume and the cosmic dilation factors in equation (11).

By equations (11) and (15), the distribution function of Q and L_{iso} is

$$P(Q, L_{\text{iso}}) = P(z, L_{\text{iso}}) \frac{dz}{dQ} = \Sigma_{\text{GRB}}(Q) \Phi(L_{\text{iso}}). \quad (18)$$

Following Langer & Norman (2006), I assume that the GRB rate is related to the SFR and the gas-phase metallicity in the host galaxy by

$$\Sigma_{\text{GRB}}(z) = A \Psi(z, \epsilon) \Sigma_{\text{SFR}}(z), \quad (19)$$

where $\Sigma_{\text{SFR}}(z)$ is the comoving rate density of star formation, $\Psi(z, \epsilon)$ is the fractional mass density belonging to metallicities below $Z = \epsilon Z_\odot$ at a given redshift z , and A is a normalization factor.

The parameter ϵ is determined by the metallicity

threshold for the production of GRBs. Studies on the GRB progenitors and the collapsar model predict that long-duration GRBs are produced only for progenitor stars with $Z/Z_\odot \lesssim 0.1$ (Hirschi et al. 2005; Yoon & Langer 2005; Woosley & Heger 2006; Yoon et al. 2006; Vink 2007). Investigations on the host galaxies of long GRBs show that an upper cut-off for the gas-phase metallicity of GRB hosts is likely $12 + \log(\text{O}/\text{H}) \sim 8.5$, corresponding to $Z \sim 0.2\text{--}0.6Z_\odot$ depending on the adopted metallicity scale and solar abundance value (Modjaz et al. 2008; see also Wolf & Podsiadlowski 2007, Savaglio et al. 2008).

In general, the stellar metallicity is always lower than the gas-phase metallicity (Gallazzi et al. 2005). Hence the two metallicity thresholds from the theoretical study on GRB progenitors and the observational investigation on GRB hosts appear to be consistent with each other. Since the metallicity evolution adopted in equation 19 and discussed in Section 3 refers to the gas-phase metallicity, throughout the paper I assume that $\epsilon = 0.3$.

According to Langer & Norman (2006),

$$\Psi(z, \epsilon) = 1 - \frac{\Gamma(\alpha + 2, \epsilon^\beta 10^{0.15\beta z})}{\Gamma(\alpha + 2)}, \quad (20)$$

where $\alpha \approx -1.16$ is the power-law index in the Schechter distribution function of galaxy stellar masses (Panter et al. 2004), and $\beta \approx 2$ is the slope in the linear bisector fit to the galaxy stellar mass-metallicity relation (Savaglio et al. 2005; Langer & Norman 2006). In equation (20), it is assumed that the average cosmic metallicity evolves with redshift by -0.15 dex per unit redshift (Kewley & Kobulnicky 2005, 2007, see eq. 7 in Section 3 and the relevant discussion).

For the SFR, Kistler et al. (2008) adopted the piecewise power-law derived by Hopkins & Beacom (2006). Here I use the the piecewise power-law derived from the updated data, given by equations (1) and (2). The two formulas differ significantly only at $z \gtrsim 4$, where measurements of the SFR are highly uncertain.

For the beaming-convolved LF of GRBs, I assume that it has a Schechter-function form

$$\Phi(L_{\text{iso}}) = \frac{1}{L_\star} \left(\frac{L_{\text{iso}}}{L_\star}\right)^{\alpha_L} \exp(-L_{\text{iso}}/L_\star), \quad (21)$$

where α_L and L_\star are constant parameters to be determined by observational data. Although people often adopt a broken power-law or a double power-law for the GRB LF (e.g., Guetta et al. 2005; Liang et al. 2007), I find that a simpler Schechter function is enough.⁴ Indeed, it appears that a power-law GRB LF at high end tends to over-produce the number of bright GRBs (B. Zhang, private communications).

⁴ Natarajan et al. (2005) and Salvaterra & Chincarini (2007) also assumed a Schechter function for the GRB luminosity in their work.

6 FITTING THE REDSHIFT DISTRIBUTION OF SWIFT GRBs

6.1 Bright GRBs

To avoid the complication of a detailed treatment of the *Swift* detector's threshold and the assumption about the GRB LF, Kistler et al. (2008) adopted a model-independent approach by selecting only GRBs with $L_{\text{iso}} > 10^{51} \text{ erg s}^{-1}$ and $z < 4$. The cut in luminosity and redshift minimizes the selection effect in the GRB data. With 36 *Swift* GRBs that satisfy the above criteria, Kistler et al. (2008) showed that the rate of GRBs increases with the redshift much faster than the SFR. A Kolmogorov-Smirnov test revealed that the SFR alone is inconsistent with the GRB rate history at the 95% level.

For GRBs with $L_{\text{iso}} > L_{\text{lim}}$, the observed number of GRBs in an observer's time interval Δt_{obs} and with Q in the interval $Q-(Q+dQ)$ is $N(Q)\Delta t_{\text{obs}}dQ$, where

$$\begin{aligned} N(Q) &\equiv \int_{L_{\text{lim}}}^{\infty} P(Q, L_{\text{iso}}) dL_{\text{iso}} \\ &= \Sigma_{\text{GRB}}(Q) \int_{L_{\text{lim}}}^{\infty} \Phi(L_{\text{iso}}) dL_{\text{iso}}. \end{aligned} \quad (22)$$

Submitting equation (21) into equation (22), one gets

$$N(Q) = \Sigma_{\text{GRB}}(Q) \Gamma\left(1 + \alpha_L, \frac{L_{\text{lim}}}{L_*}\right). \quad (23)$$

There are 45 GRBs with $L_{\text{iso}} > 10^{51} \text{ erg s}^{-1}$ in the *Swift* sample, versus the 44 GRBs in Kistler et al. (2008). The difference in the two numbers is caused by GRB 050318, whose luminosity is very close to $10^{51} \text{ erg s}^{-1}$. Kistler et al. (2008) used the isotropic-equivalent energy of GRB 050318 published in Butler et al. (2007) to calculate the luminosity and obtained a value that is slightly below the luminosity cut. As mentioned in Section 4.1, I take the isotropic-equivalent energy of GRBs from Kocevski & Butler (2007). I get a luminosity for GRB 050318 that is slightly larger than $10^{51} \text{ erg s}^{-1}$. To avoid this ambiguity arising from the luminosity uncertainty, hereafter I assume a luminosity cut $L_{\text{lim}} = 0.8 \times 10^{51} \text{ erg s}^{-1}$. Then, the total number of GRBs with $L_{\text{iso}} > L_{\text{lim}}$ is unambiguously 45.

The distribution of Q for the *Swift* 45 GRBs is plotted in Fig. 7. The additional GRB 050318 falls in the third bin, resulting that the number of GRBs in the third bin is larger by one than that in Kistler et al. (2008) (compare to their fig. 3).

Since L_{lim} is a constant, by equation (22) the number of GRBs in each equally-sized bin of Q is proportional to Σ_{GRB} , independent of the GRB LF. For the selected bright GRBs, the luminosity threshold arising from the detector flux limit has no effect when $z \lesssim 4$ (Kistler et al. 2008). Using the Σ_{GRB} given by equation (19) with Σ_{SFR} given by equations (1) and (2) (and $\alpha = -1.16$, $\beta = 2$) to fit the first six data points in Fig. 7 which have $z < 4$ by varying only the normalization, I get a surprisingly good fit as shown by the dashed curve in the figure, with $\chi_r^2 = 0.14$. This fact indicates that the GRB rate density assumed in equation (19), which takes into account the evolution of the cosmic metallicity, reasonably represents the true GRB rate. Hence, I will adopt this GRB rate density in all the following analysis.

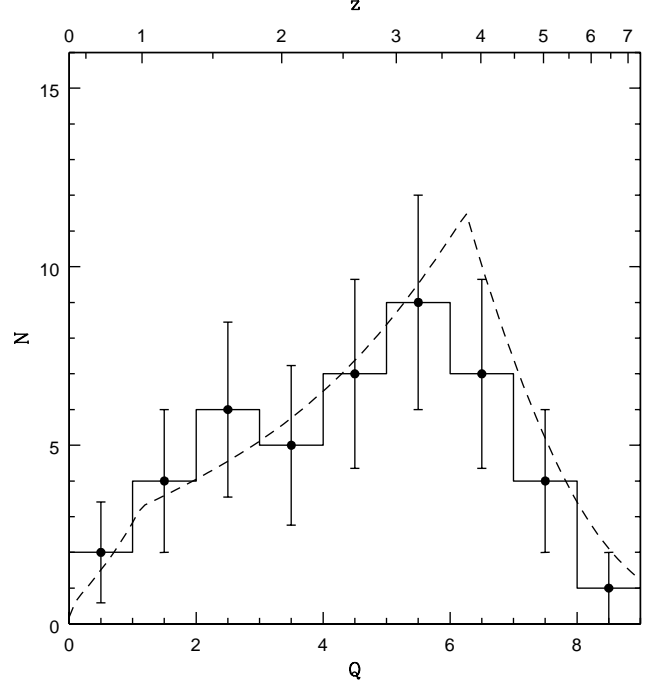


Figure 7. Distribution of Q for 45 *Swift* GRBs with $L_{\text{iso}} > 0.8 \times 10^{51} \text{ erg s}^{-1}$ (the solid histogram, with the number of GRBs in each bin indicated by a dark point with Poisson error bars). The dashed curve is the best fit of the Σ_{GRB} (eq. 19 with Σ_{SFR} given by eqs. 1 and 2) to the first 6 data points ($z < 4$) by varying the normalization, which has $\chi_r^2 = 0.14$. The deviation of the model from the data at $z > 4$ is presumably caused by the flux limit of the detector which results a decrease in the number of detected GRBs.

6.2 All GRBs

Now I consider the effect of the detector flux limit (or, equivalently, the luminosity threshold) on the distribution of luminosity and redshift for the 64 GRBs in the sample. As mentioned in Section 4.1, the observed luminosity threshold can be modeled by an energy flux limit $F_{\text{lim}} = 1.2 \times 10^{-8} \text{ erg cm}^{-2} \text{ s}^{-1}$. Then, L_{lim} is a function of z (eq. 9). The observed distribution of L_{iso} is then given by

$$\hat{\Phi}(L_{\text{iso}}) = \Phi(L_{\text{iso}}) \Delta t_{\text{obs}} \int_0^{z_{\text{max}}} f(z) dz, \quad (24)$$

where $z_{\text{max}} = z_{\text{max}}(L_{\text{iso}})$ is the maximum redshift up to which a GRB of luminosity L_{iso} can be detected, solved from equation $L_{\text{lim}}(z) = L_{\text{iso}}$.

Submitting equation (21) into equation (24) then fitting the data in Fig. 5 with $\hat{\Phi}$, I get $\alpha_L = -1.225$, $L_* = 0.986 \times 10^{53} \text{ erg s}^{-1}$, $A' \equiv \Delta t_{\text{obs}} A = 9.386$, and $\chi_r^2 = 1.18$ (the dashed curve in Fig. 5). The data excess around $L_{\text{iso}} = 3.8 \times 10^{49} \text{ erg s}^{-1}$ is at the 2.3- σ level relative to the model.⁵

The $N(Q)$ is still given by equation (23), but now L_{lim} is a function of Q . Since $-2 < \alpha < -1$, the incomplete gamma function in equation (23) can be evaluated by the

⁵ I tried also to fit the data without the outlier point. But the main results in the paper are not affected drastically.

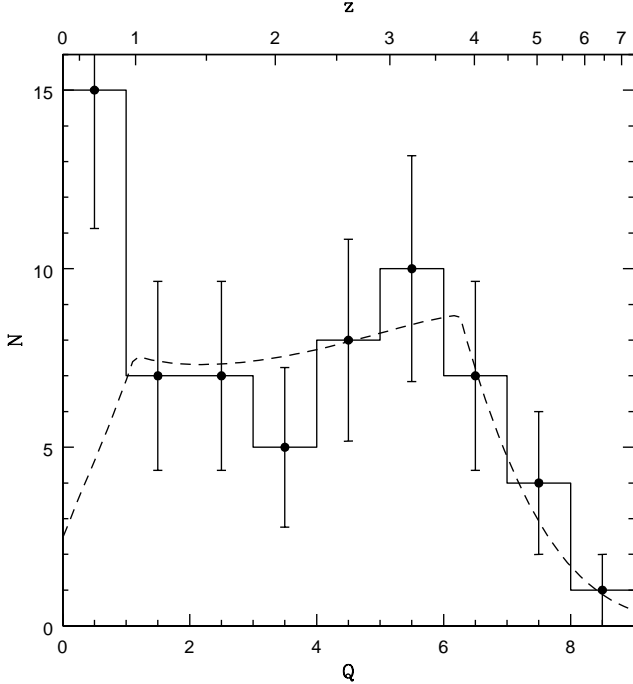


Figure 8. Distribution of Q for all the 64 *Swift* GRBs (the solid histogram, with the number of GRBs in each bin indicated by a dark point with Poisson error bars). The dashed curve shows the distribution given by equation (23) with the parameters obtained by fitting the luminosity distribution (Fig. 5, the dashed curve). The first data point has an offset about $2.7\text{-}\sigma$ from the dashed curve. The overall $\chi_r^2 = 1.01$. If the first data point is not included in the calculation of chi-squares, then $\chi_r^2 = 0.24$.

recurrence formula

$$\Gamma(a, x) = \frac{1}{a} [\Gamma(1 + a, x) - x^a e^{-x}] . \quad (25)$$

In Fig. 8, I show the distribution of Q for all the 64 *Swift* GRBs in the sample. The dashed curve is the $N(Q)$ calculated by equation (23) with the normalization and the LF parameters determined above, and L_{lim} calculated by equation (9). Globally, the modeled $N(Q)$ fits the observational data very well (without adjustment of parameters), with $\chi_r = 1.01$. However, there is an obvious excess in the number of GRBs in the bin of $0 < Q < 1$, at the $2.7\text{-}\sigma$ level. If the first bin is excluded in calculating the chi-squares, I get $\chi_r = 0.24$.

The rate of bright GRBs in equation (23) with the normalization obtained above and a constant $L_{\text{lim}} = 0.8 \times 10^{51} \text{erg s}^{-1}$ fits the first six data points ($z < 4$) in Fig. 7 with $\chi^2/\text{d.o.f} = 0.682/6$, very close to the best fit obtained by varying the normalization in Fig. 7 which has $\chi^2/\text{d.o.f} = 0.681/5$.

6.3 The Cumulative Distribution of Q

The cumulative distribution of Q for 32 *Swift* GRBs with $L_{\text{iso}} > 0.8 \times 10^{51} \text{erg s}^{-1}$ and $z < 3.5$ is shown in Fig. 9.⁶

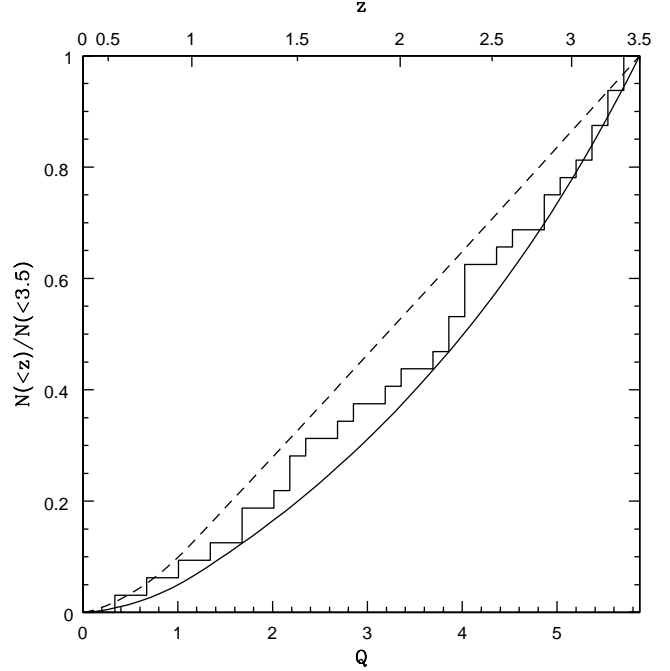


Figure 9. Cumulative distribution of $Q(z)$ for 32 *Swift* GRBs with $z < 3.5$ and $L_{\text{iso}} > L_{\text{min}} = 0.8 \times 10^{51} \text{erg s}^{-1}$ (the stepwise curve). The cut in redshift and luminosity is chosen so that the data are not affected strongly by the luminosity threshold. The smooth solid curve is calculated with the GRB rate Σ_{GRB} in equation (19), which is independent of the GRB LF. The dashed curve is calculated with the SFR given by equations (1) and (2) alone.

This subsample of GRBs is not subject to the luminosity threshold. The integral distribution of Q , defined by

$$N(< z) \equiv \int_0^{Q(z)} N(Q) dQ , \quad (26)$$

is shown with a smooth solid curve, which agrees with the observed data very well. The integral distribution of Q given by the SFR alone (the dashed curve) does not agree with the observation.

In Fig. 10, I show the cumulative distribution of Q for all the 64 GRBs in the sample. To show the excess of GRBs at low redshift, I use the cumulative distribution defined by

$$N(> z) \equiv \int_{Q(z)}^{Q(z_{\text{max}})} N(Q) dQ , \quad (27)$$

where $z_{\text{max}} = 7$. The $N(> z)$ given by the model is shown with a smooth solid curve, which fits the observed distribution beyond $z = 0.7$ very well. An excess in the number of GRBs at redshift < 0.7 is clearly seen.

Given the small number of GRBs in the sample, the observed excess in the number of GRBs at low redshift (and low luminosity, Fig. 5) could simply arise from statistical fluctuations. However, it is also possible that the excess reflects a real deviation of the redshift (and luminosity) distribution from the model, because of the following facts:

(A) The detection of highly sub-luminous and sub-energetic nearby GRBs 980425, 031203 and 060218 has led people to propose that there exists a unique population of faint GRBs, whose rate is much higher than normal cosmological

⁶ I set the upper bound of the redshift to 3.5 instead of 4 to reduce the effect of the luminosity threshold.

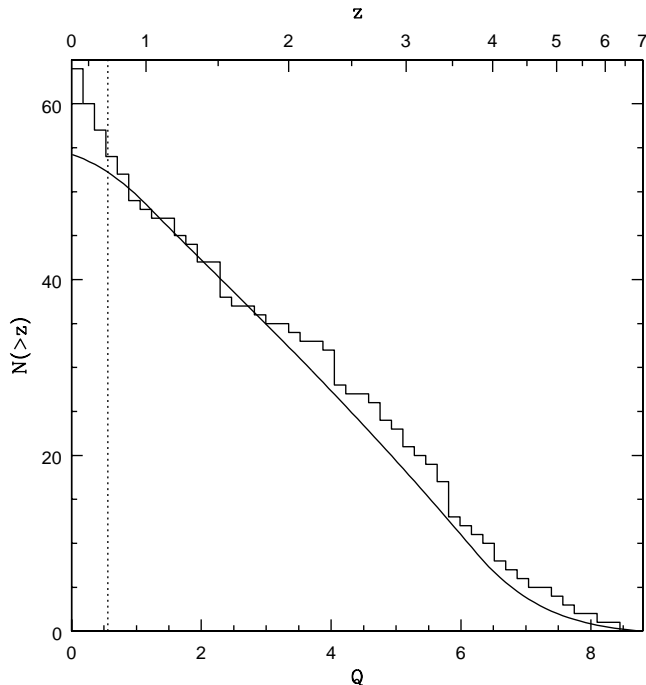


Figure 10. Cumulative distribution of $Q(z)$ for all the 64 GRBs in the sample (the stepwise curve), with $N(>z)$ defined by equation (27) ($z_{\max} = 7$). The smooth solid curve is the result given by the model. The vertical dotted line denotes $z = 0.7$ ($Q = 0.564$). An excess in the number of GRBs at $z < 0.7$ is clear (c.f. Fig. 8).

GRBs (Cobb et al. 2006a; Pian et al. 2006; Soderberg et al. 2006; Chapman et al. 2007; Guetta & Della Valle 2007; Liang et al. 2007).

(B) Some nearby long-duration GRBs are found not to have accompanied supernovae and hence are probably not related to the death of massive stars, challenging the traditional scheme for the classification of GRBs by their durations (Gehrels et al. 2006; Zhang 2006; Zhang et al. 2007a). These non-supernova GRBs include 060614 at $z = 0.125$, 060505 at $z = 0.089$ (Cobb et al. 2006b; Della Valle et al. 2006; Fynbo et al. 2006b; Gehrels et al. 2006), and 051109B at $z = 0.08$ (Perley et al. 2006).

(C) The SFH of the Local Group and other nearby galaxies indicates an excess of the local SFR density relative to the cosmic SFH in the recent epoch of $z \lesssim 0.5$ (Drozdovsky et al. 2008). This might also be a cause for the excess in the number of GRBs at $z \lesssim 0.7$.

7 CONCLUSIONS

I have presented an updated cosmic SFH up to redshift $z = 7.4$. The updated sample of SFR data are obtained by adding the new UV and IR measurements on the SFR density of Bouwens et al. (2007, 2008) and Reddy et al. (2008) to the ‘good’ data sample compiled by Hopkins & Beacom (2006). The two joined UV+IR measurements of Reddy et al. (2008) at $z \sim 2.3$ and $z \sim 3.05$ agree well with previous measurements of SFRs in the redshift interval $1 \lesssim z \lesssim 4$, and are consistent with a flat evolution SFH in this interval. The UV measurements of Bouwens et al. (2007, 2008) at $z \sim 3.8, 5, 5.9, 7.4$ and an estimate at $z \sim 10$ significantly

expand the SFR data sample at $z \gtrsim 4$, and are broadly consistent with the previous results in $3.5 \lesssim z \lesssim 6$. The updated sample provides a consistent picture for the cosmic SFH up to $z \sim 7.4$ (Fig. 3), although the dust correction at $z \gtrsim 4$ is highly uncertain which results large uncertainties in the SFH at high redshift (Drozdovsky et al. 2008).

The updated SFH still under-produces the GRB rate density at high redshift when compared to the *Swift* GRB redshift distribution (Fig. 1), confirming the previous claim (Daigne et al. 2007; Le & Dermer 2007; Kistler et al. 2008). The discrepancy is investigated under the assumption that long-duration GRBs trace both the star formation and the metallicity evolution, as motivated by the observations that long GRBs occurred in star-forming galaxies with low metallicities and the theoretical study on the collapsar model which shows that GRBs can be produced only from low-metallicity massive stars.

Since the cosmic metallicity decreases with redshift (Pettini et al. 1999; Prochaska et al. 2003; Rao et al. 2003; Kobulnicky & Kewley 2004; Kewley & Kobulnicky 2005, 2007; Kulkarni et al. 2005; Savaglio et al. 2005; Savaglio 2006), it is natural to expect that the ratio of the GRB rate to the SFR must increase with redshift if the scenario that long GRBs are produced by the death of massive stars with low metallicity (MacFadyen & Woosley 1999; MacFadyen et al. 2001; Hirschi et al. 2005; Yoon & Langer 2005; Woosley & Bloom 2006) is correct. Adopting a simple model for relating the GRB rate density to the SFR density and the cosmic metallicity evolution (Langer & Norman 2006) and assuming a flux limit for the *Swift* detector, I have shown that the redshift distribution of the 64 *Swift* GRBs with measured redshifts and calculated luminosities can be successfully fitted by the updated SFH with a threshold in the metallicity for GRB production (Figs. 7–10).

Kistler et al. (2008) have considered several possibilities for the cause of the discrepancy between the the *Swift* GRB rate and the SFH. They have shown that the Kolmogorov-Smirnov test disfavors an interpretation as a statistical anomaly. Selection effects are also not likely to cause an increased efficiency in detecting high-redshift GRBs. Although Kistler et al. have argued that alternative causes are possible (e.g., evolution in the fraction of binary systems, an evolving IMF of stars, etc), the results in this paper indicate that the cosmic metallicity evolution may be the simplest interpretation.

However, the results show an excess in the number of GRBs with low luminosity ($L_{\text{iso}} \sim 3.8 \times 10^{49} \text{ erg s}^{-1}$; Fig. 5) and at low redshifts ($z \lesssim 0.7$; Figs. 8 and 10). The existence of an excess is confirmed by the up-to-date *Swift* GRBs with measured redshifts, detected by 31 March 2008 (Fig. 11). Although it might simply be caused by statistical fluctuations, the observed excess could also be consistent with the speculation that there is a unique population of intrinsically faint and nearby GRBs (Section 6).

The GRB sample used in this paper (and in Kistler et al. 2008) is almost definitely incomplete and non-uniform, because of the complex selection biases in the redshift measurement discussed in Section 4.2. In fact, all the current works on the redshift distribution of GRBs have such a problem. However, Kistler et al. (2008) have argued that none of the selection biases appears to be able to increase

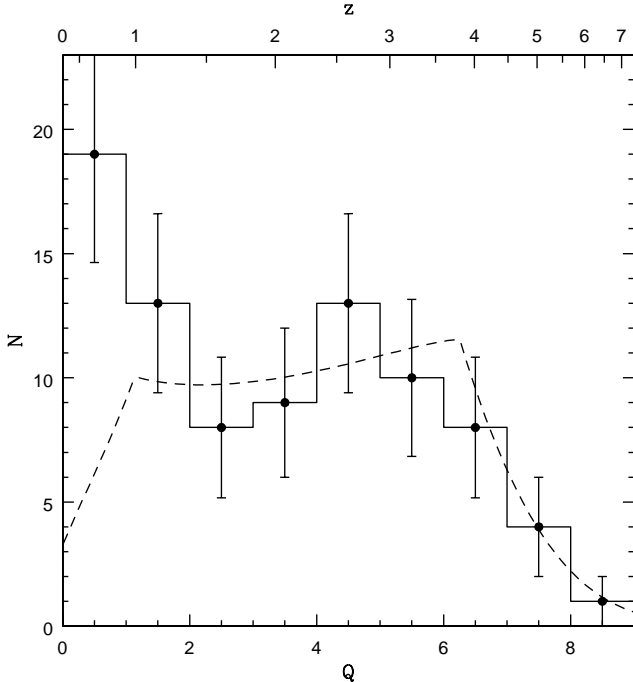


Figure 11. Distribution of Q for all the 85 *Swift* GRBs with redshifts, detected by 31 March 2008 between and including GRBs 041220 and 080330 (the solid histogram). The dashed curve shows the distribution given by equation (23) with the parameters obtained by fitting the luminosity distribution (Fig. 5, the dashed curve), renormalized by the total number of GRBs. The first data point has an offset about $3.0\text{-}\sigma$ from the dashed curve. The overall $\chi^2_r = 1.21$. If the first point is not included in the calculation of chi-squares, then $\chi^2_r = 0.28$.

the overall observability with redshift and account for the enhancement in the GRB rate relative to the SFR.

The number of GRBs in the sample is small, which also prohibits one from obtaining a strict constraint on the parameters in the GRB LF and the cosmic metallicity evolution.

Despite the above problems, the results of this work suggest that the rise of the observed *Swift* GRB rate relative to the SFR is compatible with an interpretation by the evolution of the cosmic metallicity. Once the problems are solved or significantly alleviated in future, a significantly improved and enlarged sample of GRBs with measured spectra and redshifts will become available. Then, by comparing the observed GRB rate history to the SFH determined with other approaches, it will be possible to probe the cosmic metallicity evolution with GRBs.

ACKNOWLEDGMENTS

I thank R. J. Bouwens and A. M. Hopkins for helpful communications and sharing the data used in their papers, as well as M. D. Kistler, E.-W. Liang and B. Zhang for useful communications about their works. I also thank the anonymous referee for a very enlightening report.

REFERENCES

- Adelberger K. L., Steidel C. C., Shapley A. E., Hunt M. P., Erb D. K., Reddy N. A., Pettini M., 2004, *ApJ*, 607, 226
- Band D. L., 2006, *ApJ*, 644, 378
- Berger E., Penprase B. E., Cenko S. B., Kulkarni S. R., Fox D. B., Steidel C. C., Reddy N. A., 2006, *ApJ*, 642, 979
- Berger E et al., 2005, *ApJ*, 634, 501
- Bloom J. S., 2003, *AJ*, 125, 2865
- Bloom J. S., Frail D. A., Kulkarni S. R., 2003, *ApJ*, 594, 674
- Bouwens R. J., Illingworth G. D., Blakeslee J. P., Franx M., 2006, *ApJ*, 653, 53
- Bouwens R. J., Illingworth G. D., Franx M., Ford H., 2007, *ApJ*, 670, 928
- Bouwens R. J., Illingworth G. D., Franx M., Ford H., 2008, *ApJ*, submitted (arXiv:0803.0548)
- Bromm V., Loeb A., 2002, *ApJ*, 575, 111
- Bromm V., Loeb A., 2007, to appear in “Gamma-Ray Bursts” (CUP) (arXiv:0706.2445)
- Bunker A. J., Stanway E. R., Ellis R. S., McMahon R. G., 2004, *MNRAS*, 355, 374
- Butler N. R., Kocevski D., Bloom J. S., Curtis J. L., 2007, *ApJ*, 671, 656
- Cabrera J. I., Firmani C., Avila-Reese V., Ghirlanda G., Ghisellini G., Nava L., 2007, *MNRAS*, 382, 342
- Calzetti D., Armus L., Bohlin R. C., Kinney A. L., Koornneef J., Storchi-Bergmann T., 2000, *ApJ*, 533, 682
- Campana S. et al., 2007, *ApJ*, 654, L17
- Caputi K. I. et al., 2007, *ApJ*, 660, 97
- Castro-Tirado A. J. et al., 2007, *A&A*, 475, 101
- Cen R., Fang T., 2008, *ApJL*, submitted (arXiv:0710.4370)
- Chapman R., Tanvir N. R., Priddey R. S., Levan A. J., 2007, *MNRAS*, 382, L21
- Ciardi B., Loeb A., 2000, *ApJ*, 540, 687
- Cobb B. E., Bailyn C. D., van Dokkum P. G., Natarajan P., 2006a, *ApJ*, 645, L113
- Cobb B. E., Bailyn C. D., van Dokkum P. G., Natarajan P., 2006b, *ApJ*, 651, L85
- Cole S. et al., 2001, *MNRAS*, 326, 255
- Conselice C. J. et al., 2005, *ApJ*, 633, 29
- Coward D., 2007, *New Astron. Rev.*, 51, 539
- Coward D. M., Guetta D., Burman R. R., Imerito A., 2008, *MNRAS*, in press (arXiv:0711.0242)
- Crowther P. A., 2007, *ARA&A*, 45, 177
- Crowther P. A., Dessart L., Hillier D. J., Abbott J. B., Fullerton A. W., 2002, *A&A*, 392, 653
- Daigne F., Rossi E. M., Mochkovitch R., 2007, *MNRAS*, 372, 1034
- Della Valle M. et al., 2006, *Nat*, 444, 1050
- Drozdovsky I., Hopkins A. M., Aparicio A., Gallart C., 2008, to appear in “Galaxies in the Local Volume” (arXiv:0803.2432)
- Erb D. K., Shapley A. E., Pettini M., Steidel C. C., Reddy N. A., Adelberger K. L., 2006, *ApJ*, 644, 813
- Fiore F., Guetta D., Piranomonte S., D’Elia V., Antonelli L. A., 2007, *A&A*, 470, 515
- Friedman A. S., Bloom J. S., 2005, *ApJ*, 627, 1
- Fruchter A. S. et al., 2006, *Nat*, 441, 463
- Fynbo J. P. U., Prochaska J. X., Sommer-Larsen J., Dessauges-Zavadsky M., Moller P., 2008, *ApJ*, submitted

- (arXiv:0801.3273)
- Fynbo J. P. U. et al., 2003, *A&A*, 406, L63
- Fynbo J. P. U. et al., 2006a, *A&A*, 451, L47
- Fynbo J. P. U. et al., 2006b, *Nat*, 444, 1047
- Galama T. J. et al., 1998, *Nat*, 395, 670
- Gallazzi A., Charlot S., Brinchmann J., White S. D. M., Tremonti C. A., 2005, *MNRAS*, 362, 41
- Gallerani S., Salvaterra R., Ferrara A., Choudhury T. R., 2007, *MNRAS*, submitted (arXiv:0710.1303)
- Gehrels N. et al., 2006, *Nat*, 444, 1044
- Giavalisco M. et al., 2004, *ApJ*, 600, L103
- Gorosabel J. et al., 2005, *A&A*, 444, 711
- Guetta D., Della Valle M., 2007, *ApJ*, 657, L73
- Guetta D., Piran T., 2007, *JCAP*, 07, 003
- Guetta D., Piran T., Waxman E., 2005, *ApJ*, 619, 412
- Harrison F. A. et al., 1999, *ApJ*, 523, L121
- Hirschi R., Meynet G., Maeder A., 2005, *A&A*, 443, 581
- Hopkins A. M., Beacom J. F., 2006, *ApJ*, 651, 142
- Jakobsson P. et al., 2006, *A&A*, 447, 897
- Kann D. A. et al., 2008, *ApJ*, submitted (arXiv: 0712.2186)
- Kennicutt R. C., 1998, *ARA&A*, 36, 189
- Kewley L. J., Ellison S. L., 2008, *ApJ*, in press (arXiv: 0801.1849)
- Kewley L., Kobulnicky H. A., 2005, in de Grijs R., Gonzalez Delgado R. M., eds, *Starbursts: From 30 Doradus to Lyman Break Galaxies*. Springer-Verlag, Berlin, p. 307
- Kewley L., Kobulnicky H. A., 2007, in de Jong R. S., ed, *Island Universes: Structure and Evolution of Disk Galaxies*. Springer-Verlag, Dordrecht, p. 435
- Kistler M. D., Yuksel H., Beacom J. F., Stanek K. Z., 2008, *ApJ*, 673, L119
- Kobayashi C., Springel V., White S. D. M., 2007, *MNRAS*, 376, 1465
- Kobulnicky H. A., Kewley L., 2004, *ApJ*, 617, 240
- Kocevski D., Butler N., 2007, *ApJ*, in press (arXiv: 0707.4478)
- Kulkarni S. R. et al., 1999, *Nat*, 398, 389
- Kulkarni V. P., Khare P., Péroux C., York D. G., Lauroesch J. T., Meiring J. D., 2007, *ApJ*, 661, 88
- Kulkarni V. P., Fall S. M., Lauroesch J. T., York D. G., Welty D. E., Khare P., Truran J. W., 2005, *ApJ*, 618, 68
- Lamb D. Q., Reichart D. E., 2000, *ApJ*, 536, 1
- Langer N., Norman C. A., 2006, *ApJ*, 638, L63
- Le T., Dermer C. D., 2007, *ApJ*, 661, 394
- Le Floch E. et al., 2005, *ApJ*, 632, 169
- Le Floch E., Charmandaris V., Forrest W. J., Mirabel I. F., Armus L., Devost D., 2006, *ApJ*, 642, 636
- Li L.-X., 2006, *MNRAS*, 372, 1357
- Li L.-X., 2007, *MNRAS*, 379, L55
- Liang E.-W., Zhang B., Virgili F., Dai Z. G., 2007, *ApJ*, 662, 1111
- MacFadyen A. I., Woosley S. E., 1999, *ApJ*, 524, 262
- MacFadyen A. I., Woosley S. E., Heger A., 2001, *ApJ*, 550, 410
- Mao S., Mo H. J., 1998, *A&A*, 339, L1
- Metzger M. R., Djorgovski S. G., Kulkarni S. R., Steidel C. C., Adelberger K. L., Frail D. A., Costa E., Frontera F., 1997, *Nat*, 387, 878
- Mészáros P., 2006, *Rept. Prog. Phys.*, 69, 2259
- Meurer G. R., Heckman T. M., Calzetti D., 1999, *ApJ*, 521, 64
- Modjaz M. et al. 2008, *AJ*, 135, 1136
- Nagamine K., Springel V., Hernquist L., 2004, *MNRAS*, 348, 435
- Nandra K., Mushotzky R. F., Arnaud K., Steidel C. C., Adelberger K. L., Gardner J. P., Teplitz H. I., Windhorst R. A., 2002, *ApJ*, 576, 625
- Naoz S., Bromberg O., 2007, *MNRAS*, 380, 757
- Natarajan P., Albanna B., Hjorth J., Ramirez-Ruiz E., Tanvir N., Wijers R., 2005, *MNRAS*, 364, L8
- Nuza S. E., Tissera P. B., Pellizza L. J., Lambas D. G., Scannapieco C., de Rossi M. E., 2007, *MNRAS*, 375, 665
- Ouchi M. et al., 2004, *ApJ*, 611, 660
- Paczynski B., 1998, *ApJ*, 494, L45
- Panther B., Heavens A. F., Jimenez R., 2004, *MNRAS*, 355, 764
- Pérez-González P. G. et al., 2005, *ApJ*, 630, 82
- Perley D. A., Foley R. J., Bloom J. S., Butler N. R., 2006, *GCN* 5387
- Péroux C., Dessauges-Zavadsky M., D'Odorico S., Kim T.-S., McMahon R. G., 2007, *MNRAS*, 382, 177
- Pettini M., Ellison S. L., Steidel C. C., Bowen D. V., 1999, *ApJ*, 510, 576
- Pian E. et al., 2006, *Nat*, 442, 1011
- Piran T., 2004, *Rev. Mod. Phys.*, 76, 1143
- Porciani C., Madau P., 2001, *ApJ*, 548, 522
- Price P. A., Cowie L. L., Minezaki T., Schmidt B. P., Songaila A., Yoshii Y., 2006, *ApJ*, 645, 851
- Prochaska J. X., Gawiser E., Wolfe A. M., Castro S., Djorgovski S. G., 2003, *ApJ*, 595, L9
- Prochaska J. X. et al., 2004, *ApJ*, 611, 200
- Prochaska J. X., Chen H.-W., Dessauges-Zavadsky M., Bloom J. S., 2007, *ApJ*, 666, 267
- Prochter G. E. et al., 2006, *ApJ*, 648, L93
- Rao S. M., Nestor D. B., Turnshek D. A., Lane W. M., Monier E. M., Bergeron J., 2003, *ApJ*, 595, 94
- Reddy N. A., Steidel C. C., 2004, *ApJ*, 603, L13
- Reddy N. A., Steidel C. C., Pettini M., Adelberger K. L., Shapley A. E., Erb D. K., Dickinson M., 2008, *ApJS*, 175, 48
- Rol E. et al., 2007, *ApJ*, 669, 1098
- Salpeter E. E., 1955, *ApJ*, 121, 161
- Salvaterra R., Chincarini G., 2007, *ApJ*, 656, L49
- Savaglio S., 2006, *New J. Phys.*, 8, 195
- Savaglio S., Glazebrook K., Le Borgne D., 2008, *ApJ*, submitted (arXiv:0803.2718)
- Savaglio S. et al., 2005, *ApJ*, 635, 260
- Schaefer B. E., 2007, *ApJ*, 660, 16
- Schiminovich D. et al., 2005, *ApJ*, 619, L47
- Soderberg A. M. et al., 2004, *ApJ*, 606, 994
- Soderberg A. M. et al., 2006, *Nat*, 442, 1014
- Stanek K. Z., Garnavich P. M., Kaluzny J., Pych W., Thompson I., 1999, *ApJ*, 522, L39
- Stanek K. Z. et al., 2006, *Acta Astron.*, 56, 333
- Stanway E. R., McMahon R. G., Bunker A. J., 2005, *MNRAS*, 359, 1184
- Steidel C. C., Adelberger K. L., Giavalisco M., Dickinson M., Pettini M., 1999, *ApJ*, 519, 1
- Steidel C. C., Shapley A. E., Pettini M., Adelberger K. L., Erb D. K., Reddy N. A., Hunt M. P., 2004, *ApJ*, 604, 534
- Sudilovsky V., Savaglio S., Vreeswijk P., Ledoux C., Smette A., Greiner, J., 2007, *ApJ*, 669, 741
- Tanvir N. R., Levan A. J., 2007, to appear in the proceed-

- ings of “070228: The next decade of GRB afterglows”,
Amsterdam March 2007 (arXiv:0709.0861)
- Totani T., 1997, ApJ, 486, L71
- Totani T., Kawai N., Kosugi G., Aoki K., Yamada T., Iye
M., Ohta K., Hattori T., 2006, PASJ, 58, 485
- van Paradijs J. et al., 1997, Nat, 386, 686
- Vink J. S., 2007, A&A, 469, 707
- Vink J. S., de Koter A., 2005, A&A, 442, 587
- Vreeswijk P., Ellison S., Wijers R., Hjorth J., 2004, Nucl.
Phys. B (Proc. Suppl.), 132, 295
- Wainwright C., Berger E., Penprase B. E., 2007, ApJ, 657,
367
- Watson D. et al., 2007, ApJ, 652, 1011
- Wijers R. A. M. J., Bloom J. S., Bagla J. S., Natarajan,
P., 1998, MNRAS, 294, L13
- Wolf C., Podsiadlowski P., 2007, MNRAS, 375, 1049
- Wolfe A. M., Gawiser E., Prochaska, J. X., 2005, ARA&A,
43, 861
- Woosley S. E., Bloom J. S., 2006, ARA&A, 44, 507
- Woosley S. E., Heger A., 2006, ApJ, 637, 914
- Yan H. et al., 2005, ApJ, 634, 109
- Yoon S.-C., Langer N., 2005, A&A, 443, 643
- Yoon S.-C., Langer N., Norman C., 2006, A&A, 460, 199
- Yüksel H., Kistler M. D., 2007, Phys. Rev. D, 75, 083004
- Zhang B., 2006, Nat, 444, 1010
- Zhang B., Mészáros P., 2004, Int. J. Mod. Phys., 19, 2385
- Zhang B., Zhang B.-B., Liang E.-W., Gehrels N., Burrows
D. N., Mészáros P., 2007a, ApJ, 655, L25
- Zhang B. et al., 2007b, Nat, 444, 1010

This paper has been typeset from a \LaTeX file prepared
by the author.